United Nations Educational, Scientific and Cultural Organization
GRÓ GTP Geothermal Training Programme Under the auspices of UNESCO

GRÓ GTP, Grensásvegur 9,
IS-108 Reykjavík, Iceland

Reports 2021
Number 16

BUTAJIRA GEOTHERMAL PROSPECT IN SILTI ZONE, SOUTHERN-ETHIOPIA: 1D JOINT INVERSION OF MT AND TEM RESISTIVITY DATA – GEOLOGICAL AND GEOTHERMAL SIGNIFICANCE

Kebede Mengesha Negatu
Geological Survey of Ethiopia (GSE)
Geothermal Resource Exploration and Evaluation Directorate
P.O. Box 2302
Addis Ababa
ETHIOPIA
kebedeme29@gmail.com

ABSTRACT

Resistivity surveying including MT and TEM is an important geophysical method in geothermal energy exploration and other research work. An MT/TEM survey was conducted in the Butajira geothermal prospect in Ashute, S-Ethiopia, where 38 collocated MT and TEM soundings were carried out in 2017 and 2019. The data were processed and 1D jointly inverted. Here, the results are presented as vertical cross-sections and depth-slices (horizontal cross-sections) and the results compared to previous geological and other geothermal findings.

The resistivity structure of Butajira geothermal prospect, Ashute area, is characterized by conductive shallow lying resistivity layers (<5-10 Ωm) with an average thickness of about 1,200 to 1,600 m. The conductive layers reach down to a depth of 200 to 600 m a.s.l. The subsurface is composed of volcanic sediments including lithified ash, fine- to coarse-grained sandstone, well laminated conglomerate and debris or lahar. The clasts consist mostly of pyroclastic material derived from a silicic center in the south. The low resistivity is probably caused by saline sediments or smectite due to low temperature hydrothermal alteration, but most likely a combination of both. Below the low-resistivity layers there is high resistivity with values higher than 70 Ωm.

The high resistivity below the conductive zone is believed to reflect major fault systems, the tectonic trend of the Debre zait Silti rift graben and the Main Ethiopian Rift (MER). Geothermal fluid from depth rises to shallow levels most likely along a NE-SW discontinuity and NW-SE structures. It flows laterally and enriches the shallow permeable formation and appears as thermal surface manifestations.

Electrical strike analyses of the MT data, using the vertical component of the magnetic field for different frequencies (depth levels), are in good agreement with the 1D resistivity model and support it.

In the future, it is recommended to add more MT and collocated TEM soundings in the north and west of the Ashute field to define the resistivity structure better, as well as performing TEM soundings at the same location as the already existing MT sites to correct for static shift of the MT data. Finally, detailed geological mapping of the area is proposed, in particular tectonic mapping and gravity surveying to delineate geological structures.

1. INTRODUCTION AND BACKGROUND

Exploration for geothermal resources in Ethiopia within and close to the rift margin has been carried out by the Ethiopian Government and the United Nation Development Program (UNDP) since 1969 and regional exploration activities have been undertaken by both national and international organizations (UNDP, 1973). Geological mapping of Ethiopia has been performed for the whole rift at a scale of 1:500,000. Geological, geochemical and geophysical results are available from 16 geothermal prospect areas in the rift and later, additional explorations were conducted. Currently, the prospect areas in Ethiopia are believed to be around 24, and the estimated power potential more than 10,000 MWe (Kebede, 2016).

The prospects are at different exploration and exploitation stages. In addition to the surface exploration studies, a semi detailed surface exploration of ten sites in the central and southern Afar was carried out by the Geological Survey of Ethiopia (GSE) and Electroconsult (ELC, 1986). In the 1980s, eight exploratory wells were drilled in the central sector of the Main Ethiopian Rift (MER), in Aluto Langano and Tendaho in Afar. The wells in Aluto Langano were productive and produced 7.3 MWe. Recently two appraisal trajectory wells were added. Tulu Moye – Gedemsa, Tendaho, Meteka, Corbetti, Abaya, Dofan and Fantale are a few of the prospect areas in which detailed exploration studies have been performed, and drilling is planned or has been started (Abera Kebede, 2021).

The Butajira prospect in Silti Ashute area is located on the western margin (escarpment) of the MER (Figure 1). Previously, geothermal exploration was focused on the rift and the eastern part of the active fault system of the MER, particularly on the Wonji fault system in both the Southern and Northern Afar rift. The Butajira project area was recommended in the United Nations Development Programme technical report for further detailed geological and geochemical studies (UNDP, 1973). The area was regarded as a low-enthalpy geothermal resource that could be used for direct use rather than electricity generation. In April 2014, there was an explosion of hot thermal fluid during deep drilling of an irrigation well (Abera Kebede and Mulugeta, 2017). This potentially hazardous situation changed previous views about the area and led to more detailed exploration work. A part of that entailed measuring 38 MT (Magnetotelluric) and TEM (Transient Electromagnetic) soundings. The Butajira geothermal project work started with geological, geophysical, and geochemical research in March 2017 (Wondifra Tadesse, 2018). A geophysical survey using the MT resistivity method was performed in the Ashute area from April 10th, 2017 to May 27th, 2017. During this period 32 MT soundings were made, of which 4 were of very bad data quality. The remaining 28 MT soundings were processed and 1D inverted, creating a resistivity model of the area (Wondifra Tadesse, 2018). The data were not static shift corrected as no TEM data existed at that time. In 2019 additional 10 MT and 38 collocated TEM soundings were measured.

Resistivity methods are the most important geophysical methods in geothermal subsurface exploration studies (Hailegiorgis Abebe, 2018). The reason is that the resistivity is highly sensitive to temperature and geothermal alteration processes and is directly related to the parameters characterizing the reservoir (Hersir et al., 2022). Therefore, the main emphasis here is placed on the description of the resistivity methods and resistivity of rocks.

This report will focus on two of the most important active and passive electromagnetic resistivity methods in geophysical exploration:

- The transient electromagnetic method (TEM) which is an active method; and
- The magnetotelluric method (MT) which is a passive method.

1D joint inversion of MT and TEM data from the Butajira prospect area and surroundings in the SW (southwest) part of the MER was carried out and the results are presented as resistivity maps and cross-sections.

1.1 The objectives of the study

The objective of the MT and TEM survey was to acquire high-quality resistivity data from the survey area to: (i) static shift correct the MT data using TEM data and obtain a more reliable model of the subsurface resistivity structure of the Butajira prospect, Ashute geothermal field, and (ii) estimate the probability of occurrence, extension and depth of the geothermal reservoir and possible recharge zones of the system. The scope of the study includes data acquisition, processing, 1D joint inversion of MT and TEM data by using the temtd program to construct a model which presents the results followed by discussion, conclusion and recommendation. This means updating the already existing resistivity model based on the 28 MT soundings (Mengiste et al., 2018; Wondifra Tadesse, 2018) as there have now been added 10 MT and 38 collocated TEM stations.

1.2 Location of the study area

The Butajira geothermal field is in the western margin (escarpment) of the Central Main Ethiopian Rift (CMER) that extends from Afar (northeast part of Ethiopia) to Mozambique in the south. Butajira town is located 135 km south of Addis Ababa. The geophysical survey area is around 20 km southeast of Butajira town, the total distance from Addis Ababa is about 155 km. Morphologically, the prospect can be categorized into two areas (Abera Kebede and Mulugeta, 2017). The first one is the western escarpment area that is covered by pyroclastic deposits, flood basalts, basement rocks and the vertical cliffs of a high mountain range rising more than 2,500 m a.s.l. The second one is the rift floor, which is covered by talus deposits, fan deposits, alluvial and colluvial deposits, lacustrine sediments and surface geothermal manifestations (hot springs, mud pools, occasional geysers and geothermal grass) (Abera Kebede and Mulugeta, 2017). Hydro-geologically, the prospect is rich in groundwater resources that drain from the rift shoulder and the escarpment area. These areas are believed to be the major source of recharge to geothermal reservoirs in the rift floor. The quaternary sediments in the rift floor serve as an impermeable cap to a convective heat flow system in the basin as seen in Figure 1 (Abera Kebede and Mulugeta, 2017).

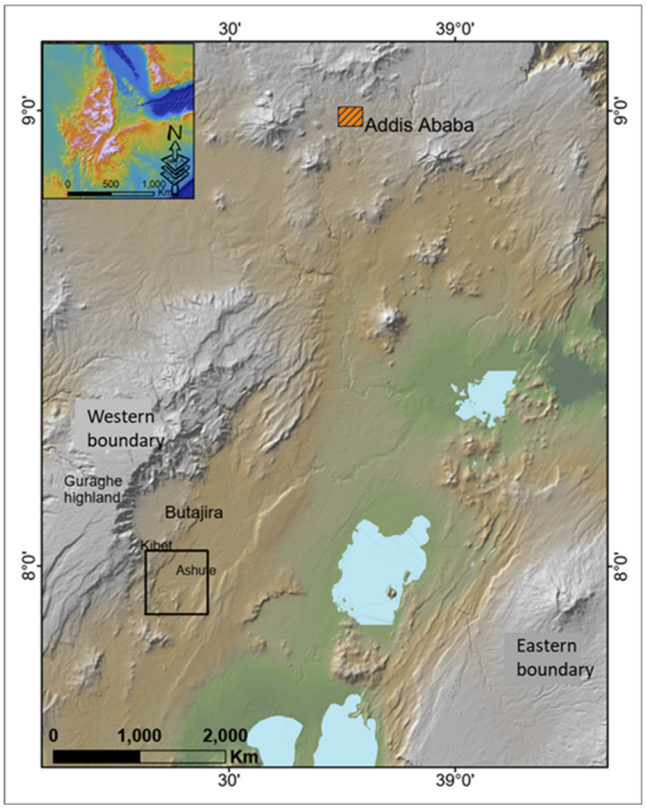

FIGURE 1: Location map of the study area (shown in the black square) and surroundings. The inset map shows the Afar triple junction

2. GEOLOGY AND TECTONIC SETTING OF THE STUDY AREA

The East African Rift System (EARS) is one of the greatest rift systems on earth. It is divided into a relatively old volcanically active part, the Eastern branch, and a younger, less active part, the Western branch. The stage of rifting in the northern branch of the EARS shows northward progression from the immature stage in Tanzania to more advanced rifting in Kenya and an incipient sea floor spreading stage in Afar and the MER (Abera Kebede, 2021). The MER (Figure 2) is a part of the Eastern branch of the EARS connecting the Kenya rift to the Afar triple junction, separating the plateaus into the

western/Ethiopian and eastern/Somalian plateaus (Mohr, 1983). It is categorized into three main segments, the northern, central, and southern segments (Mohr, 1983; WoldeGabriel et al., 1990). The northern segment extends from the Afar triple junction southward to Lake Koka, while the central sector extends from the Lake Koka area to Lake Awasa, where the rift margin changes its direction and turns from NE-SW, approximately, to N-S. The southern MER extends further up to the Turkana depression, the northern limit of the Kenyan rift (Abera Kebede, 2021).

The Butajira volcanic area is a part of the CMER situated on the western boundary (Figure 1 and 2). The CMER is of Late Miocene-Early Pliocene age (5/6-7 Ma). It is characterized by ~N25°E to N30°E orientation and steeply dipping boundary faults that have a large vertical offset of more than 1,500 m (Boccaletti et al., 1998). The volcanic and tectonic activity in the CMER is confined to the marginal areas. The eastern margin is characterized by the Asela-Langano fault system at the rift margin and the Wonji fault system on its floor (Figure 2). The Wonji fault system shows signs of Pleistocene-Holocene magmatic and tectonic activity, defined by the magmatic segments that obliquely cut the rift floor (Abebe et al., 2007; WoldeGabriel et al., 1990). The magmatic segments are made of N-NNE striking normal faults and central volcanoes. The activity in the western margin is expressed by the volcanic zones (Butajira-Silti and Debrezeyit; Figure 2). N-NNE aligned Quaternary cinder cones and fissures define the volcanic zones (Abebe et al., 2007). The western boundary is characterized by the Fonko and Guraghe fault escarps.

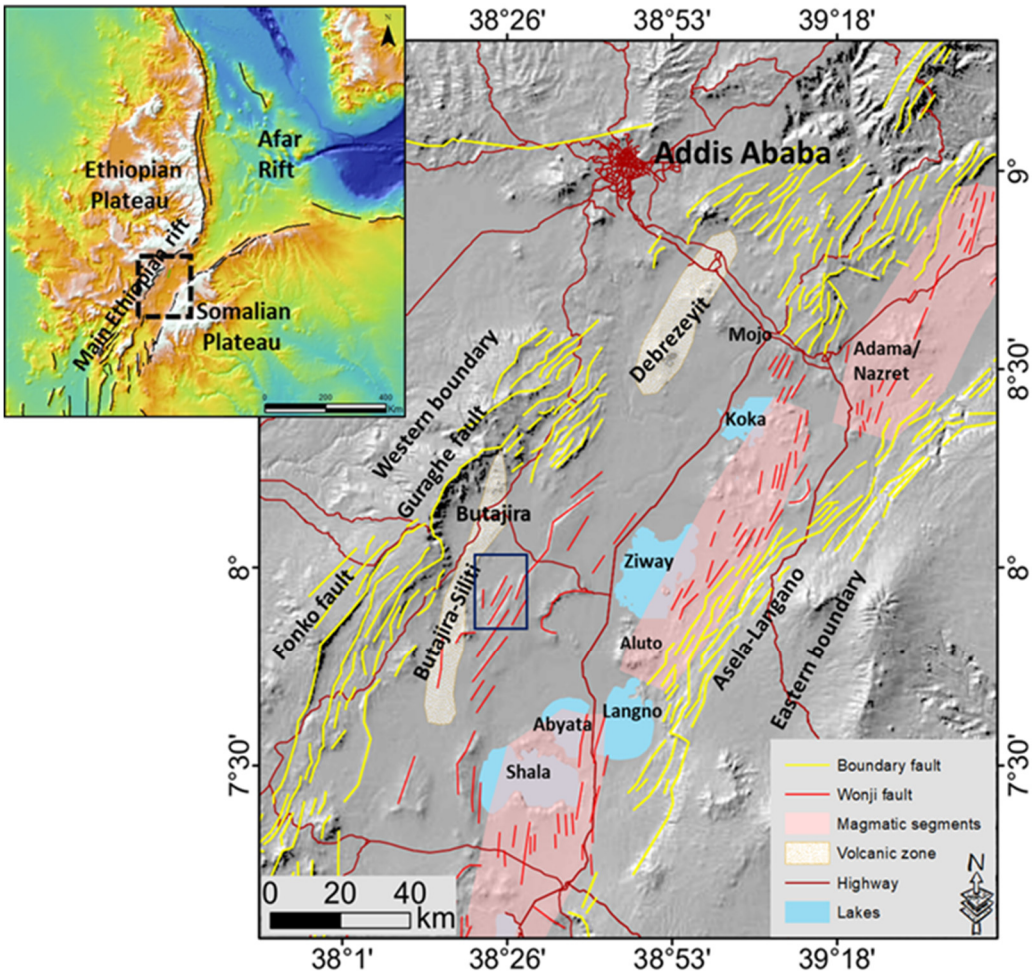

FIGURE 2: Tectonic map of the CMER and location of the study area (indicated in the blue rectangular box). The inset map shows a Digital Elevation Model (DEM) of Ethiopia. Modified from Abera Kebede (2021)

Lithologically, the rocks in the study area and its surrounding are characterized by Late Miocene–Pleistocene ignimbrites, Oligocene flood basalts and basement rocks, Pliocene–Pleistocene trachytic lava flows, plateau pyroclastic fall, and flow deposits (Figure 3; Abebe et al., 2017). Down from the western escarpment, also called 'Butajira-Silti', the volcanic field consists of a large group of basaltic cinder cones, maars, and lava flows dominantly trending in NE-SW direction (Abebe et al., 2007). The flat lain area, east of the Guraghe fault escarp, is mainly characterized by secondary products of the escarpment: talus deposits, fan deposits, alluvial and colluvial deposits mixed with some lacustrine deposits (Abebe et al., 2017).

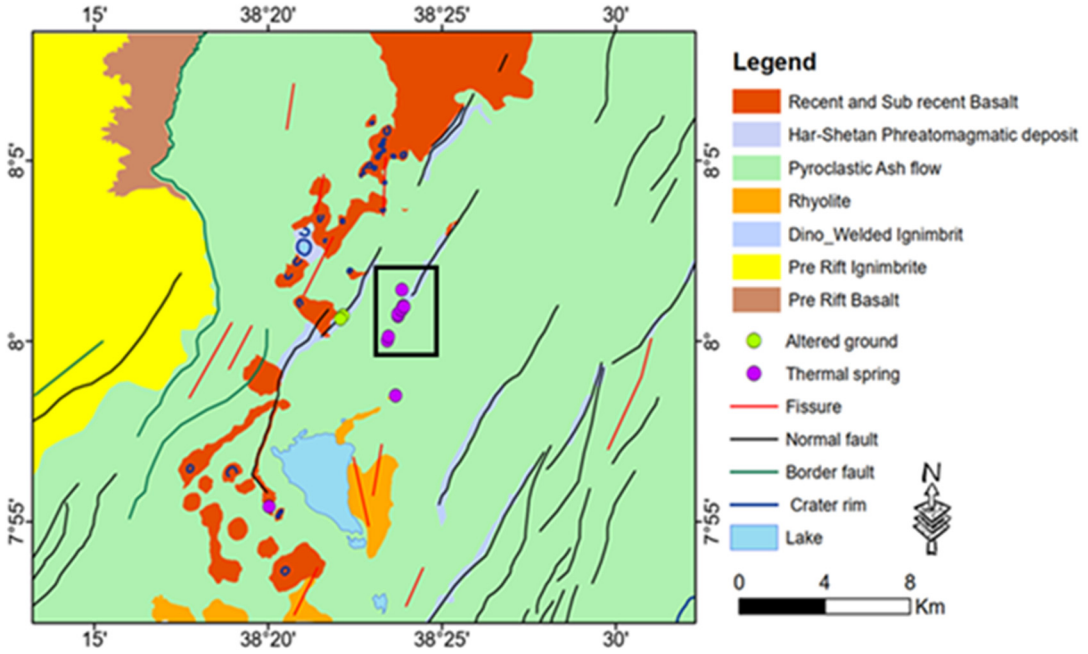

FIGURE 3: Geological and structural map of the Butajira-Silti area, indicating the most pronounced tectonic features, geological structures, and surface manifestations. The study area is within the black rectangular box. Modified from Abebe et al. (2017)

The study area is marked by normal faults and fissures of different orientations. These are NE-SW to N-S oriented borders and major faults as well as NNE-SSW oriented fissures and faults (Figure 3). Some hidden structures could also be identified from a shallow temperature survey (Abera Kebede and Mulugeta, 2017). Geothermal surface manifestations are observed following the orientation of the main fracture direction (Abera Kebede and Mulugeta, 2017).

3. RESISTIVITY OF THE SUBSURFACE AND THE RESISTIVITY METHOD

3.1 Resistivity of rock

Electrical resistivity is defined through Ohm's law:

$$\boldsymbol{E} = \rho \boldsymbol{j} \tag{1}$$

where $\boldsymbol{E}$ = Electrical field [V/m];
ρ = Electrical resistivity [Ωm]; and
$\boldsymbol{j}$ = Current density [A/m^2].

In geothermal fields, the resistivity of rocks is affected by the salinity and temperature of the pore fluid, the porosity of the rock, saturation level of the pores, alteration of the rock and degree of melting of the host rock (Árnason et al., 1987; Hersir and Árnason, 2009; Hersir et al., 2022).

3.2 Porosity, permeability, and pore structure of the rock

Resistivity decreases with increasing porosity of the host rock and increases with decreasing porosity according to *Archie's law* (Archie, 1942):

$$\rho = \rho_w a/\Phi^n \tag{2}$$

Where ρ = Bulk resistivity [Ωm];
ρ_w = Resistivity of the pore fluid [Ωm];
a = An empirical parameter, varies from <1 for intergranular porosity to >1 for joint porosity, usually around 1;
Φ = Porosity in proportions of total volume [0-1]; and
n = Cementing factor, an empirical parameter, usually around 2.

3.3 Salinity of the water in the rock pore spaces

Resistivity decreases linearly with increasing salinity of the pore fluid and increases linearly with decreasing salinity in the pore fluid; ρ ≈ 10/concentration in g/L of NaCl (Keller and Frischknecht, 1966).

3.4 Temperature of the pore fluid

At moderate temperatures (0-200°C), resistivity of an aqueous solution decreases with increasing temperature due to increasing mobility of the ions caused by a decrease in viscosity of the pore fluid (Dakhnov, 1962). However, at temperature above 300°C, the same process increases fluid resistivity (Quist and Marshall, 1968).

Dakhnov's relationship shows that:

$$\rho_w = \frac{\rho_{w0}}{1 + (T - T_0)} \tag{3}$$

where ρ_w = Pore fluid resistivity [Ωm] at temperature T [°C];
ρ_{wo} = Pore fluid resistivity [Ωm] at reference temperature T_0 [°C]; and
T_0 = Reference temperature [°C].

The factors that can significantly change the bulk resistivity of a rock in a hydrothermal environment are effective porosity of the rock matrix, salinity of the pore fluid, temperature, and hydrothermal alteration. In the instance where hot groundwater comes into contact with the rock, the surface that is in direct contact with the hot fluid is subject to secondary mineralization. This is often referred to as hydrothermal alteration. It has a relevant effect on the conductivity of the altered rock. Different types of alteration minerals vary depending on the temperature of the water coming into contact with the rock. Figure 4 shows the range of temperature values at which different alteration materials are formed. The alteration minerals have different conductivities leading to a different bulk resistivity of the rock matrix.

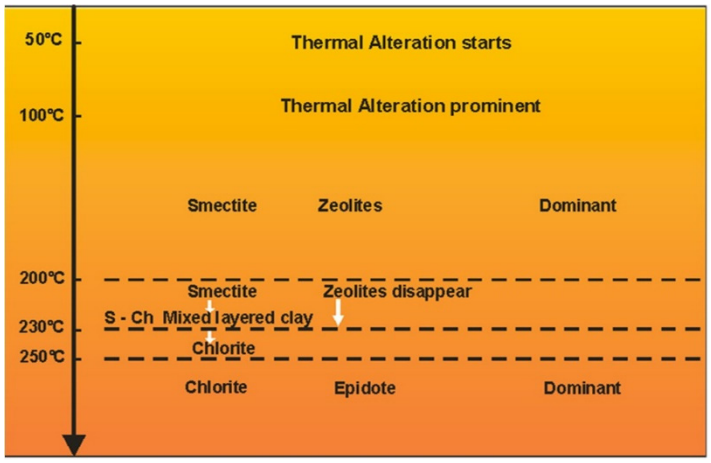

FIGURE 4: Temperature versus the different alteration minerals (Hersir and Árnason, 2009)

3.5 Water-rock interaction and alteration mineralogy of the host rock

The alteration mineralogy controls the subsurface resistivity structure in high temperature geothermal areas where the host rocks are volcanic. A shallow lying conductive caprock is found in these high temperature areas with considerable amounts of smectite, a conductive low temperature alteration mineral that has a high cation exchange capacity (CEC) (Hersir et al., 2022). Underneath, there is a core of high resistivity (geothermal reservoir) (Figure 5). The transition from the low-resistivity cap to the high-resistivity core coincides with a change in mineral alteration, that is from smectite to mixed-layered clays, chlorite and epidote which are formed at temperatures close to 230°C in basaltic geothermal systems (Kristmannsdóttir, 1979). The difference in conductivity between the smectite and the chlorite/epidote alteration zones is attributed by the difference in CEC. Smectite has a much higher CEC (0.8-1.5 meq g^{-1}) than the chlorite-epidote (0.01meq g^{-1}). Hence, conductivity is higher in the conductive cap than in the resistive core which is dominated by chlorite/epidote alteration minerals (Hersir et al., 2022). The relationship between the subsurface resistivity, hydrothermal alteration, temperature and conduction mechanism is summarized in Figure 5. It is important to note that the altered rocks tend to preserve the resistivity anomalies even if they have cooled down since the alteration process took place. Sometimes the alteration minerals indicate lower temperatures than observed in wells. This might be caused by a lack of circulating hot geothermal fluid which is necessary for hydrothermal alteration to take place, or it is a young system being heated up and the alteration is lagging behind. Thus, finding the resistivity anomalies of a typical high-temperature geothermal system does not guarantee the existence of a hot geothermal system (Hersir et al., 2022).

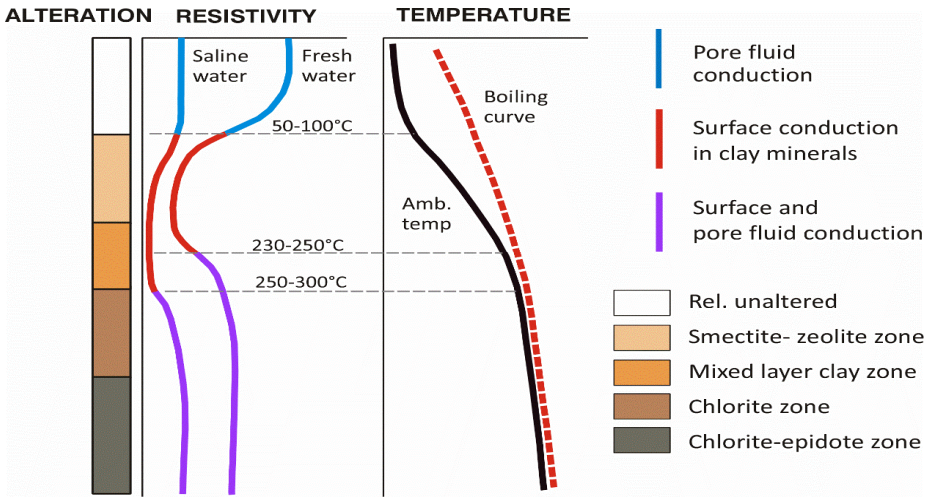

FIGURE 5: The generalized resistivity structure of a high-temperature geothermal field in volcanic environment (Flóvenz et al., 2012, modified from Flóvenz et al. (2005))

3.6 Resistivity methods

The MT and TEM resistivity methods are the most powerful, important and most recent subsurface geophysical exploration methods for geothermal resources. This is because the method images the variations of resistivity of the subsurface rocks and resistivity is closely linked to the parameters that describe geothermal system (Didas, 2018).

3.7 Basic electromagnetic theory and Maxwell's equations

The theory of electromagnetic induction is described through Maxwell's equations, shown below (Chave et al., 2012). Maxwell's equations are four equations which give a complete description of the relationship between electric and magnetic fields in any medium:

$$\boldsymbol{\nabla} \times \vec{H} = \vec{J} + \frac{\boldsymbol{\partial}\vec{D}}{\boldsymbol{\partial t}} \qquad \text{Ampere's Law} \qquad (4)$$

$$\boldsymbol{\nabla} \times \vec{E} = -\frac{\boldsymbol{\partial}\vec{B}}{\boldsymbol{\partial t}} \qquad \text{Faraday's Law} \qquad (5)$$

$$\boldsymbol{\nabla} \cdot \vec{D} = \eta \qquad \text{Gauss's Law for electricity} \qquad (6)$$

$$\boldsymbol{\nabla} \cdot \vec{B} = 0 \qquad \text{Gauss's Law for magnetism} \qquad (7)$$

where $\vec{B}$ = Magnetic induction [T];
$\vec{H}$ = Magnetic field intensity [A/m];
$\vec{D}$ = Electric displacement [C/m^2];
$\vec{E}$ = Electrical field [V/m];
η = Electric charge density of free charges [C/m^3]; and
$\vec{J}$ = Electric current density [A/m^2].

Equation 4 says that circulating magnetic fields are produced by the vector sum of electric currents density and variable electric fields (Ampere's law) and Equation 5 states that circulating electric fields are produced by variable magnetic fields (Faraday's law). The electric field diverges from electric charges and the net outflow of the electric field through any closed surface is proportional to the charge enclosed by the surface (Gauss's law of electricity) which is given in Equation 6. Equation 7 states that there are no magnetic monopoles (Gauss's law of magnetism).

It can be shown that the relationship between the electric and magnetic field in a given medium can be expressed by the following equation:

$$\begin{bmatrix} E_x \\ E_y \end{bmatrix} = \begin{bmatrix} Z_{xx} & Z_{xy} \\ Z_{yx} & Z_{yy} \end{bmatrix} \begin{bmatrix} H_x \\ H_y \end{bmatrix} \qquad (8)$$

Or in matrix notation:

$$\vec{E} = Z\vec{H} \qquad (9)$$

where $\vec{E}$ and $\vec{H}$ are the electric and magnetic field vectors (in the frequency domain), respectively, and Z is a complex impedance tensor which contains information about the subsurface resistivity structure (Hersir et al., 2022). The values of the impedance tensor elements depend on the resistivity structure below and around the site. For a 1D Earth, $Z_{xy}=-Z_{yx}$ and $Z_{xx}=Z_{yy}=0$. For a 2D Earth, that is, resistivity varies with depth and in one principal horizontal direction, it is possible to rotate the coordinate system by mathematical means, such that $Z_{xx}=Z_{yy}=0$, but $Z_{xy}\neq-Z_{yx}$. For a 3D Earth, all elements of the impedance tensor are different (Hersir et al., 2022).

3.8 Skin depth (depth of penetration)

An estimated quantitative measure of the penetration depth of an electromagnetic wave into a conductive medium can be expressed by Equation 10. The penetration depth (δ) is the depth where the electromagnetic wave has attenuated to a value of e^{-1} of its surface amplitude (about 0.37). The depth of penetration increases with increasing period, T, of the wave and increasing resistivity in the subsurface. The depth of penetration is called the "skin depth". This means that a resistive medium can be investigated to much greater depth than a conductive medium.

$$\delta \approx 500\sqrt{\rho T} \tag{10}$$

where δ = Skin depth [m];
ρ = Resistivity [Ωm]; and
T = Period [s].

3.9 Homogeneous Earth

In a homogeneous Earth, electromagnetic waves propagate such that the electric and magnetic fields are orthogonal and the ratio of the electric to the magnetic field is directly related to the apparent resistivity of the penetrated media. Applying Equation 8, the following relationship can be derived (Keller and Frischknecht, 1966):

$$\rho(T) = 0.2T \left|\frac{\boldsymbol{E_x}}{\boldsymbol{B_y}}\right|^2 = 0.2T \left|\frac{\boldsymbol{E_y}}{\boldsymbol{B_x}}\right|^2 \tag{11}$$

where E is in mV/km, B is in nT (B=μH; where μ is the magnetic permeability), and T is in s.

3.9.1 1D Earth

Depending on its variations, the resistivity of the Earth can be described by three different types of resistivity models: 1D, 2D and 3D. These are explained in the following sub-chapters.

A 1D layered Earth model (Figure 6) assumes that the half space is flat, composed of many layers and each layer is characterized by a uniform conductivity (Ward and Wannamaker, 1983).

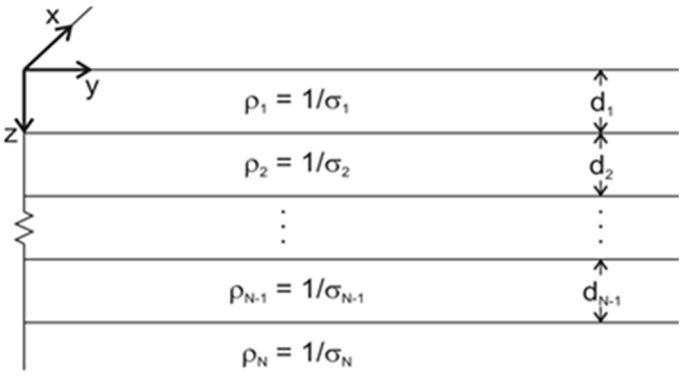

FIGURE 6: N-layered Earth showing resistivity variations with depth, a 1D model (Ward and Wannamaker, 1983)

In 1D interpretation, it is assumed that the resistivity varies only with depth. Thus, the diagonal elements of the impedance tensor, Z_{xx} and Z_{yy}(which couple parallel electric and magnetic fields components), are zero while the off-diagonal components (which couple orthogonal electric and magnetic field components) are equal in magnitude but have opposite signs (Chave et al., 2012; Hersir et al., 2022).

3.9.2 2D Earth

In 2D interpretation it is assumed that resistivity varies along one of the two principal horizontal directions as well as with depth. In case of a 2D homogeneous Earth, Z_{xx} and Z_{yy} are equal in magnitude, but have opposite signs, while Z_{xy} and Z_{yx} are different (Chave et al., 2012).

3.9.3 3D Earth

The real Earth is best described by a 3D model where resistivity varies in all three directions ($\rho(x, y, z)$). In a 3D homogeneous Earth model, all the components of the impedance tensor are non-zero and the diagonal elements Z_{xx} and Z_{yy} do not become zero simultaneously in any coordinate system. Likewise, the off-diagonal elements of the impedance tensor Z_{xy} and Z_{yx} differ. Thus, when interpreting a 3D Earth model, all tensor elements are considered (Chave et al., 2012).

3.9.4 The problem of MT measurements and the dead band

The so-called **"**dead band" in MT is the frequency band between 0.5 and 5 Hz of the natural magnetic field amplitude spectrum (Figure 7). This band is characterized by low-amplitude signals. The spectrum is caused by the interaction between the Earth's magnetic field generated by magneto-hydrodynamic processes within the Earth's outer core and extra-terrestrial magnetic fields generated by the solar wind in the ionosphere. It is attributed to inductive source mechanisms, one effective above ~1 Hz, the other below ~1 Hz, and it frequently manifests in MT sounding curves by a reduction in data quality (Chave et al., 2012; Flóvenz et al., 2012). Unfortunately, the remedy for this problem in MT data has not yet been discovered. Thus, the processed data are always of low quality in the dead band frequency range. A similar local minimum or "dead band" is also observed for frequencies between 1 and 5 kHz (AMT).

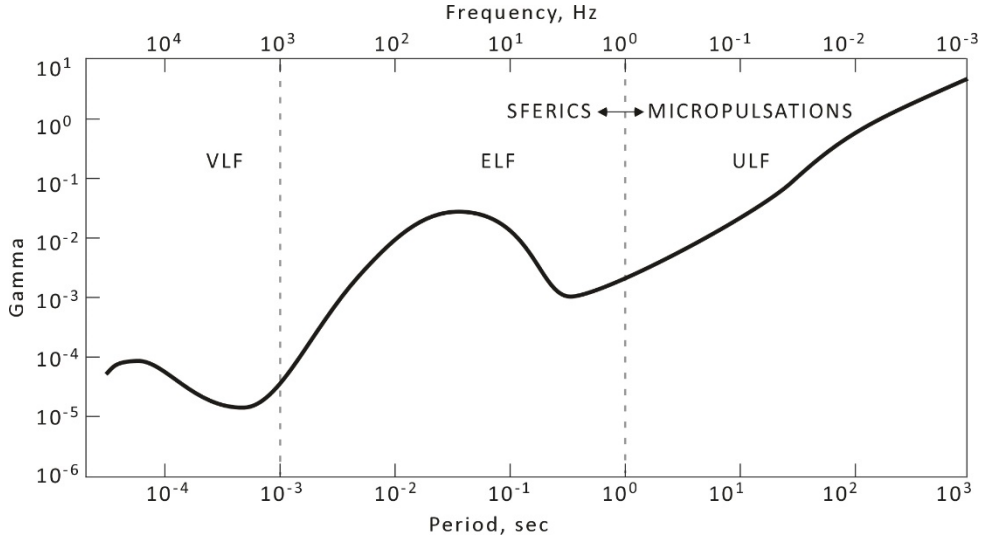

FIGURE 7: The mean natural magnetic field amplitude spectrum in gammas ($\gamma = nT$) as a function of the period (Flóvenz et al., 2012)

4. METHOD

4.1 Data acquisition and geophysical exploration technique

The MT method is a passive electromagnetic (EM) exploration method that measures the natural electric ($\vec{E}$) and magnetic field ($\vec{H}$) in perpendicular directions on the surface of the Earth to determine the electrical behaviour of the Earth. The MT method is used to evaluate the subsurface resistivity structure of the earth down to several hundred meters and even a few kilometers depending on the period and the resistivity structure under the site (Hersir et al., 2022). In the MT method, two types of frequency ranges are used for data acquisition: high frequency which is used to resolve shallow lying structures and low frequency to detect deep subsurface structures. Figure 8 shows the Phoenix V5 2000 MT equipment and Figure 9 shows the standard set-up of an MT measurement.

4.2 MT survey – instrumentation

The MT resistivity survey in Butajira was carried out in two phases. The first phase was from April 10th, 2017 to May 27th, 2017. During this period, 32 MT soundings were measured. Of the 32 soundings, 4 soundings were of very bad data quality and cannot be processed. Therefore, it was decided

FIGURE 8: Phoenix geophysics equipment V5 2000 MT system (Phoenix, 2018)

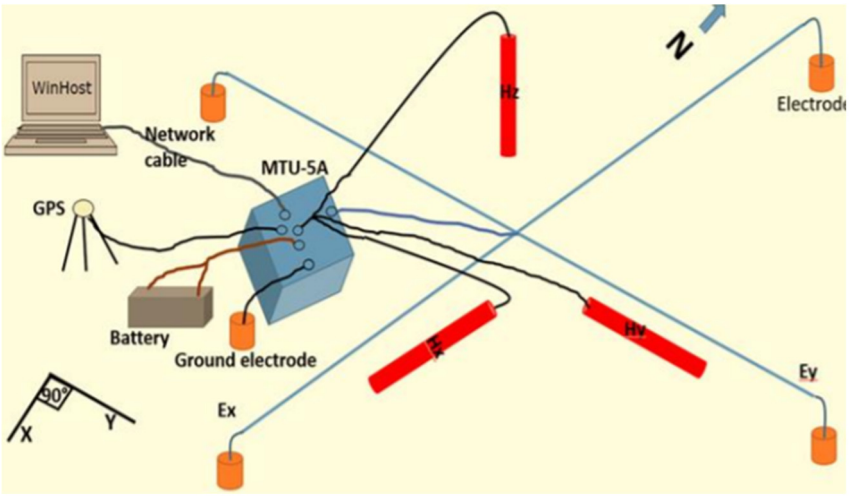

FIGURE 9: The standard layout of an MT set-up (Hailegiorgis Abebe and Hersir, 2020)

to use only 28 MT stations which had already been processed by Wondifra Tadesse (2018). The second phase took place in March 2019. Then, additional 10 MT soundings and 38 collocated TEM soundings were measured. An MT data acquisition system from Phoenix Geophysics Ltd Company in Canada was used. The instruments used for the MT survey consist of a data logger (MTU-5A) and two pairs of electric dipoles, E_x and E_y, for measuring the electric field in X and Y direction, respectively. The X direction was aligned N-S and the Y direction E-W. Three magnetics coils are connected by magnetic cables for measuring the time variations of the natural magnetic field ($\vec{H}$) in the X, Y and Z direction (H_x, H_y, H_z). Accessories consisted of a battery, compact flash card, GPS and five non-polarizable pots; four pots are used for measuring E_x and E_y and the last one was for ground connection. The pots were filled with lead chloride solution in a ceramic container that is designed to ensure a good contact with the ground (see Figure 9).

4.3 Processing of MT time series (TS) data

Data processing generally involves several stages as shown in Figure 10. The processing steps were mostly carried out using the software Synchro time series viewer (TS), SSMT2000, and MTEditor from Phoenix Geophysics (2005). When we have acquired the data from the field, we first download and copy the data from the compact flash. After that we can roughly visualize the data in the synchronise time series viewer and after that we apply the SSMT2000 and process the TS (Time series), transforming the data from the time domain to the frequency domain. We then process the data with robust and non-robust processing techniques and conduct reference processing if reference data are available. When

we process using reference data, the cross-power data according to our choice consisted of 40 segments and were edited to minimize the noise and the standard deviation to enhance continuous apparent resistivity and phase data (Phoenix, 2005).

When we finish the processing using SSMT200 we get two files which contain the high frequency and the low frequency part of the data acquisition (*.mth and *.mtl), respectively. Those two files serve as input files for the MTEditor software (Figure 11). We can now plot these two files in the MTEditor as apparent resistivity and phase versus frequency and edit them. The editing is either done manually or automatically (Didas, 2018). After finishing the editing, the file is saved as *.mpk file and finally exported to the standard file format *.edi (electronic data interchange) to make it readable by standardized inversion software like temtd, and WinGLink.

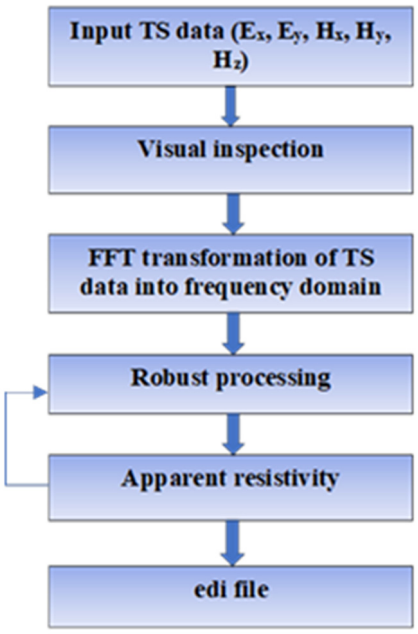

FIGURE 10: Data processing flow chart

The MT/TEM survey in Butajira, Ashute prospect area, was conducted along 19 profiles covered by 38 stations. The spacing is shown in Table 1: the profiles stretch over the area of the geothermal surface manifestations and are oriented nearly perpendicular to the general regional geological trend, which is in NE-SW direction (Figure 12). The distance between profiles is around 1 to 1.5 km and the stations are about 1 to 1.5 km or more apart. In Ashute, the profiles are laid out as infill profiles close to the surface manifestations (Table 1) because the data quality was not good.

An example of MT data processing is shown in Figure 13. Figures showing the MT data processing of all MT soundings can be found in Appendix I in the Appendices report (Mengesha Negatue, 2021).

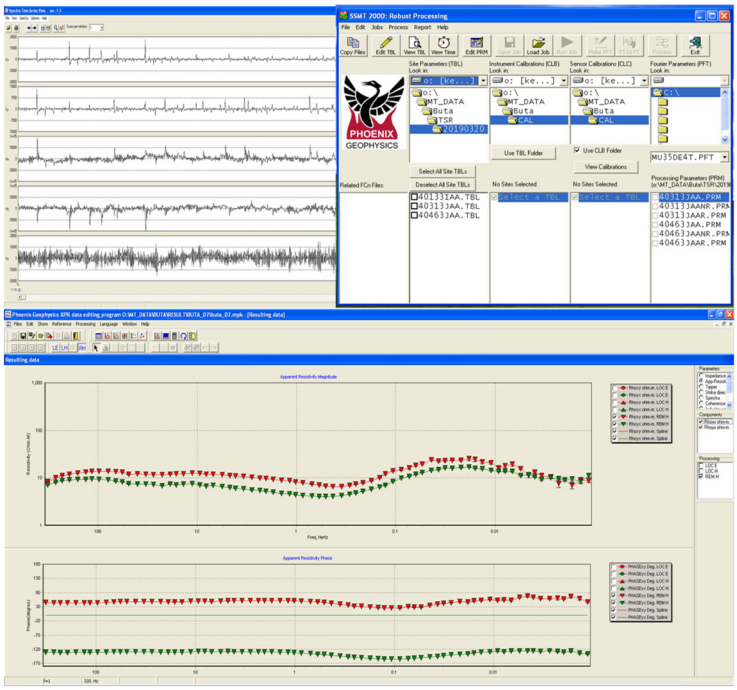

FIGURE 11: From raw MT data to apparent resistivity and phase curves for both polarizations. Above: Synchro time series viewer (left) and SSMT2000 menu (right) Below: MTEditor

TABLE 1: Summary of the MT and TEM survey

Geophysical method	Data type	Distribution measurement	Profile station interval (km)	Profile interval (km)	Total sounding
Magnetotellurics (MT)	Single reading at single sounding	Parallel profiles	1-1.5	1-3 or ≤1	38
Transient electromagnetics (TEM)	Single reading at single sounding	Parallel profiles	1-1.5	1-3 or ≤1	38

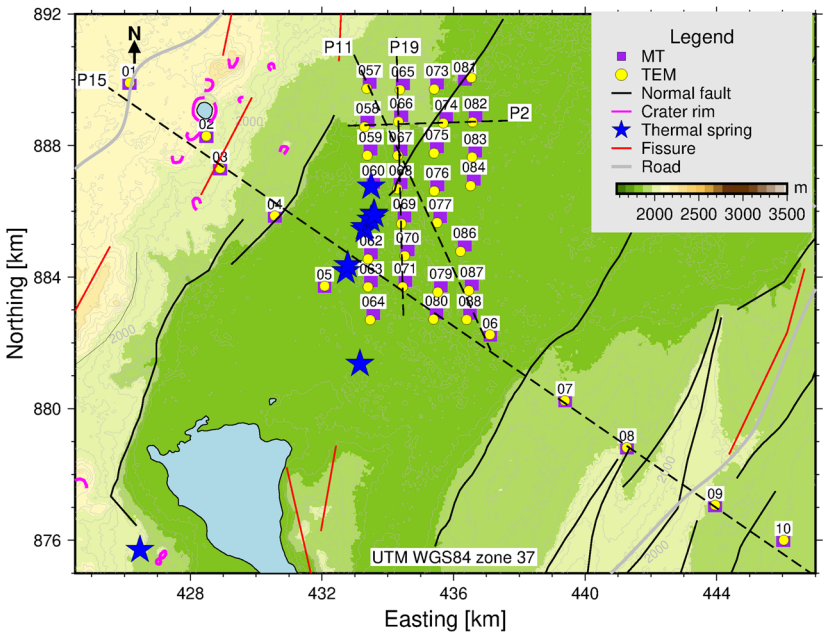

FIGURE 12: Location of MT (purple square) and TEM soundings (yellow circle), and the resistivity profiles. Blue stars show geothermal manifestations. An A (Ashute) in front of all the names of MT and TEM stations has been dropped on the figure to make it more readable

4.5 TEM survey - instrumentation

The TEM method is an active electromagnetic method. TEM measurements allow geophysical exploration from a few tens of meters below the surface to several hundreds of meters (see Árnason (1989) for details). The depth of resolution in TEM measurements depends on the subsurface resistivity, the induced current, receiver sensitivity, and transmitter-receiver geometry (size of the transmitter loop). Acquiring TEM data for Butajira was done for static shift correction of MT data.

The TEM measurement setup consists of a transmitter, transmitting loop, and a receiver – a vertical magnetic coil or antenna (Figure 14). Data acquisition in TEM works as shown in Figure 14. A constant artificial current is transmitted through the transmitter loop of wire, which is laid on the ground (size of the loop is 100 m x 100 m) and a constant magnetic field of known strength is built up (Árnason, 1989) as shown to the right in Figure 14. During the data acquisition time, the transmitter and the receiver are communicating or synchronized by GPS (Global Positioning System) for the receiver to know when the transmitter turns off and on. For Zonge GDP-32 TEM, the measurements were made using three transmitting frequencies of 16, 8 and 1 Hz. In this work the Zonge GDP-32 equipment was used.

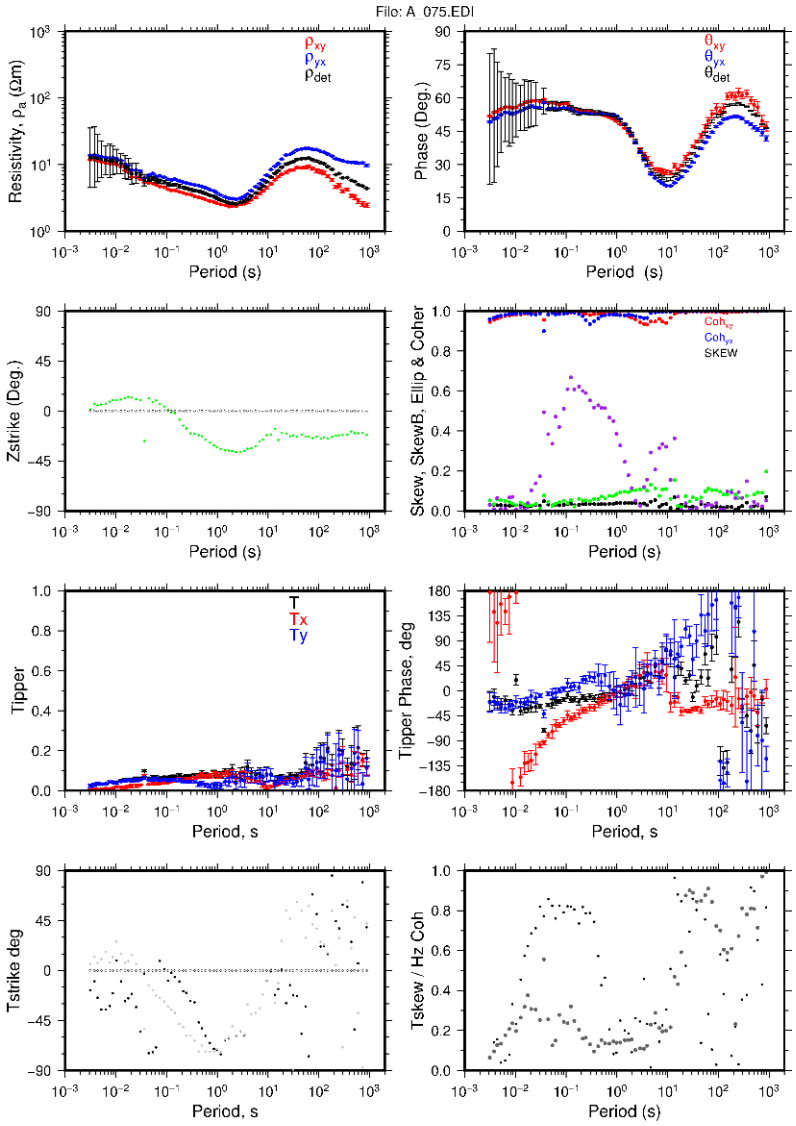

FIGURE 13: Example of processed MT data (station number A075); the apparent resistivity and phase: ρ_{xy} (in red) and ρ_{yx} (in blue), and ρ_{det} (in black) which is calculated from the determinant of the impedance tensor. Z-strike, skew, ellipticity, Tipper and coherency are shown as well (Mengesha Negatue, 2021)

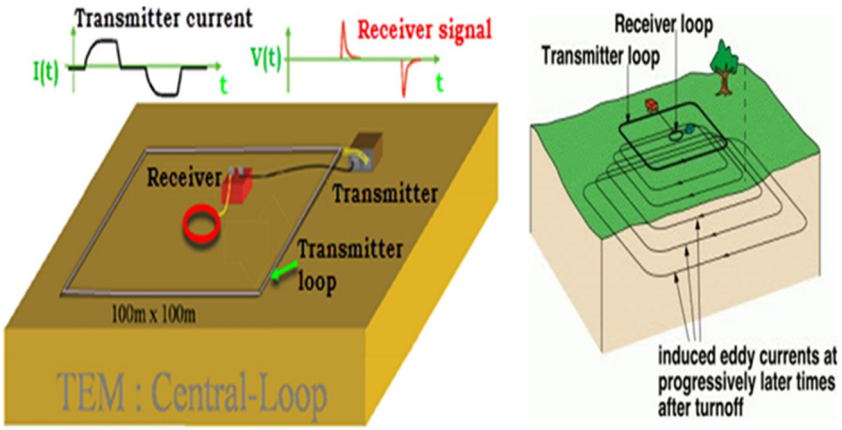

FIGURE 14: TEM measurement layout demonstrating how the method works (Zonge, 2018)

4.6 Processing TEM raw data using the TemX program

First, the raw/measured TEM data are downloaded from the Zonge GDP-32 TEM acquisition system and converted to *.USF file format by using the manufacturer software. The Zonge raw data are kept as *.CAC files as produced by the Zonge receiver. The data are then converted to *.AVG format using the 'TEMAVGW" program and then to *.USF format using the "TEMTRIM" program. The *.USF files are the input files for the TemX program written at ÍSOR (Árnason, 2006a). The TemX program reads and processes the standard file format of the central loop TEM data. It performs normalization of the voltages with respect to the transmitted current, gain and effective area of the antenna and then displays all the data graphically, allowing the user to omit outliers. It calculates averages of the data set and the time apparent resistivity. The program produces an output file *.inv ready for inversion in programs such as temtd, which is explained in the following chapter.

4.7 1D inversion

Temtd is a 1D inversion program which is used to find a horizontally layered Earth resistivity model based on TEM and MT data. The program was developed at ÍSOR in 2006 (Árnason, 2006b). It can invert MT and TEM data separately or jointly. The temtd software is written in ANSI-C, runs under LINUX or UNIX operating systems and uses the gnu plot graphics program for graphical display during the inversion process. The program can be used to perform both layered Earth and Occam inversion of fixed thickness of the layers which increases exponentially with depth. In this project the Occam inversion was applied (Figure 15).

The processed result of a TEM sounding is expressed as an apparent resistivity ρ_a (or more correctly the so-called late-time apparent resistivity) as a function of the square root of time after the current turn-off. The current turn-off at late times after the induced currents have diffused way below the surface, and the response is independent of near-surface conditions.

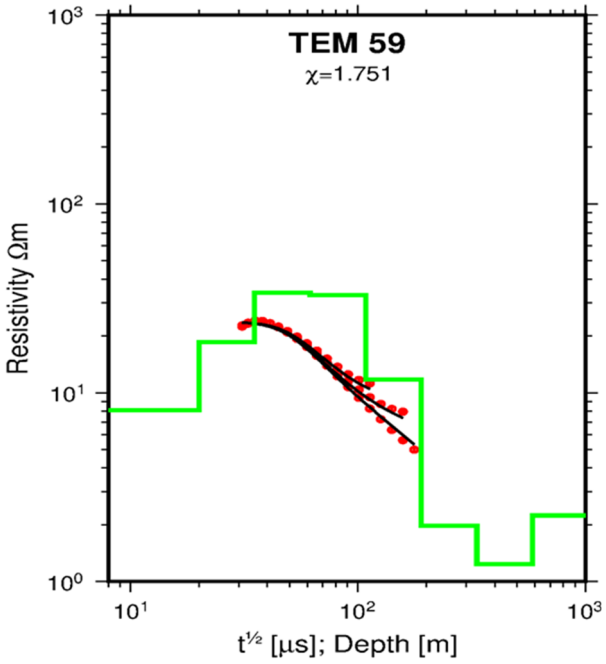

FIGURE 15: TEM sounding data from the Ashute geothermal area, apparent resistivity for three frequencies 16 Hz, 8 Hz, and 1 Hz as a function of the square root of time after the current turn off and the associated 1D Occam model. Red dots are the measured late-time apparent resistivities for the three frequencies and the black line is the apparent resistivity calculated from the model shown in green. At the top of the figure is the misfit function; the root-mean-square difference between the measured and calculated values, χ=1.751

5. RESULTS AND INTERPRETATION

5.1 1D joint inversion

The location of all 38 MT and TEM soundings used for inversion in this work is shown in Figure 12. The MT data were collected in a collaboration between the Geological Survey of Ethiopia and the Faculty of Earth Science of Addis Ababa University applying the MTU-5A MT units from Phoenix Geophysics while the TEM data were acquired using a Zonge GDP-32 unit. A 100 m × 100 m square transmitter loop was applied, and a central receiver was used, measuring the vertical component of the magnetic field.

The 1D joint inversion of MT and TEM data in this study was done using the temtd software. All the 1D joint inversion models are presented in Appendix II in the Appendices report (Mengesha Negatue,

2021). Several rotational invariants exist for 1D inversion of MT data and the question arises which apparent resistivity/phase curve to invert for. This is discussed by Park and Livelybrooks (1989) and here the apparent resistivity and phase calculated from the determinant value of the impedance tensor was used. The first layer of the initial model was assigned a fixed thickness of 10 m and the half-space was given a constant resistivity value between 10 and 30 Ωm. For most of the inversions, an initial model with 30 layers was used except for three stations. Damping factors were applied to smoothen the output model until the best model was found. The misfit of the model was evaluated by the chi-square factor. The highest chi-square error in the final fit was 9.45, most of the errors were less than 2 (see Appendix II in Mengesha Negatue (2021)). The static shift multiplier was one of the parameters in the inversion which shifted the MT data up and down. An example of 1D joint Occam inversion of MT and TEM data is shown in Figure 16.

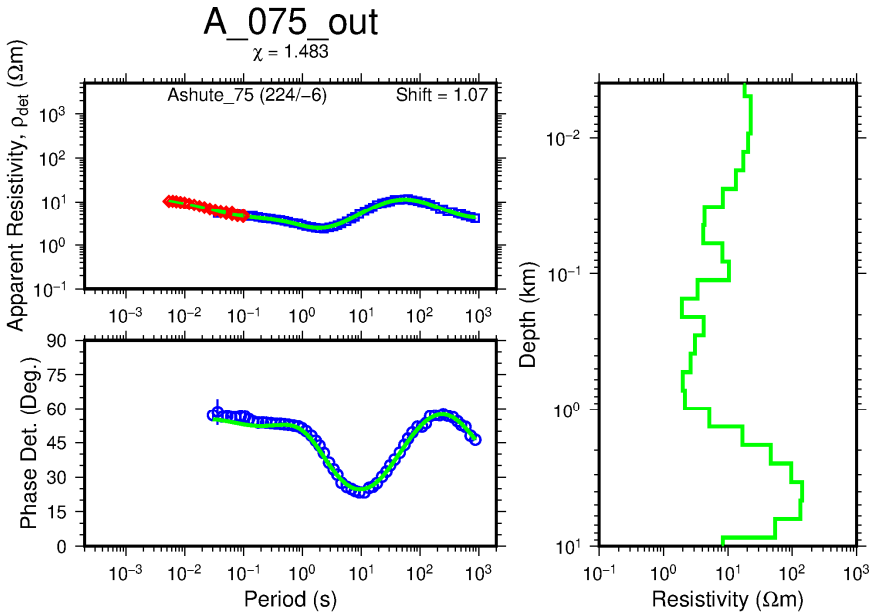

FIGURE 16: An example of the result of joint 1D Occam inversion of MT and TEM data. TEM apparent resistivity (red diamond), blue square and circle are measured apparent resistivity and phase, respectively, derived from the determinant of the MT impedance tensor, vertical blue lines are error bars. Green lines show the response of the model calculation on the right panel. The phase response number (224/6) indicates that two stations of MT and TEM were 224 m apart and their elevation difference was 6 m. In accordance with Figure 16, A_075 is the name of an MT station and Ashute_75 is the name of a TEM station. The static shift correction was 1.07 and the root mean square difference between the measured and calculated value was χ=1.483. The maximum depth was around 6 km

5.2 Static shift multipliers

Static shift in MT is caused by shallow resistivity heterogeneities close to the sounding site and manifests itself in parallel shift of the apparent resistivity over the whole range of frequencies (Chave and Smith, 1994).

The static shift multiplier for the 38 MT soundings was calculated using the rotationally invariant apparent resistivity calculated from the determinant value of the impedance tensor through joint inversion with data from the collocated TEM soundings. The spatial distribution of the multipliers is shown in Figure 17. The multipliers were in the range of 0.6-1.1, most commonly around 0.9 (Figure 18). In the static shift correction of MT data, the apparent resistivity values are divided by the shift multiplier. From the histogram (Figure 18), we can see that most of the soundings were shifted up (shift

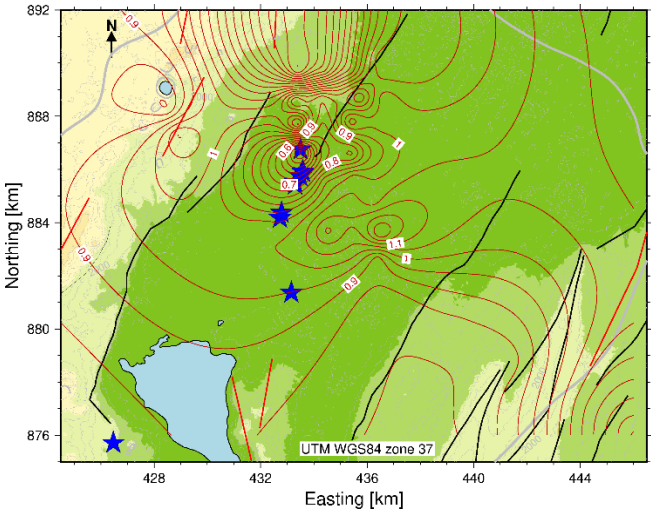

FIGURE 17: Spatial distribution of the static shift multipliers. Blue stars are surface manifestations, black lines are the inferred faults mapped on the surface and red lines are the fissures

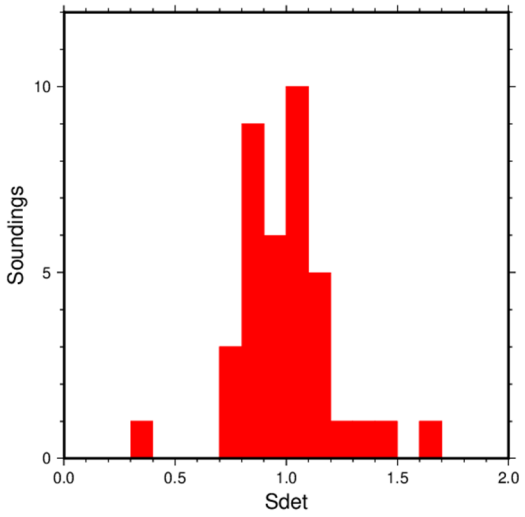

FIGURE 18: Histogram of static shift multipliers for the MT soundings

factor <1) and only a few shifted down (shift factor >1). The biggest static shift multipliers are observed southeast and northwest of the Ashute area where shallow-subsurface alluvial sediments are found. Low static shift multipliers are observed around the surface mani-festation area at low topography where steep slopes are likely to have strong distortion effects on the telluric currents.

5.3 Resistivity cross-sections

The 1D inversion results are presented here as vertical and horizontal pseudo 2D resistivity cross-sections (resistivity maps). The vertical cross-sections were generated using the TEMCROSS program (Eysteinsson, 1998). All the resistivity cross-sections compiled from the 1D models are displayed in Appendix III in the Appendices report (Mengesha Negatu, 2021). The depth of resolution of the 1D models differs from sounding to sounding because of different data quality (the acquired useable long periodic data). This is reflected in different depth resolution of the cross-sections. Most of the resistivity cross-sections indicate resistivity structures down to a depth of 3-6 km. The location of the cross-sections is displayed in Figure 12 and four of them are discussed in this report to emphasize the main results of the 1D joint inversion (Figure 19-22). They are given down to two depths: 1,000 and 4,000 m b.s.l.

5.4 Vertical resistivity cross sections

Here, four vertical cross-sections are shown and discussed; their locations are given in Figure 12. Resistivity cross-section along profile 2 (Figure 19) is located south of Butajira and west of Aluto Langano, close to the western margin of the MER. It lies from west to east and crosses the southeast dipping NE-SW trending inferred thrust fault. The main visible features are:

- A well-defined conductive cap of 1-10 Ωm with thickness of about 1,400 m, starting at a depth of about 300 m below the surface and reaching down to 1,700 m below the surface.
- A moderately resistive zone of 10-100 Ωm below the conductive layer with a thickness of about 1,500 m.
- A thick resistive zone (> 100 Ωm) extending from between 1,000 and 1,700 m b.s.l. to great depths.

Resistivity cross-section along profile 11 (Figure 20) runs NW-SE across the regional geological structures of the rift fault. Its location is given in Figure 12.

- A well-defined conductive cap of 1-10 Ωm with thickness of about 1,000 to 1,400 m reaches to the surface close to the surface manifestations and the main fault.
- A 10-30 Ωm low resistivity layer with thickness at around 400 to 800 m is located right below the conductive cap.
- A moderately resistive zone of 30-70 Ωm is seen below the conductive layer. A resistive zone of 70-100 Ωm is found below the low resistivity.
- A very resistive zone of 100-200 Ωm domes up between station 66 and 77.

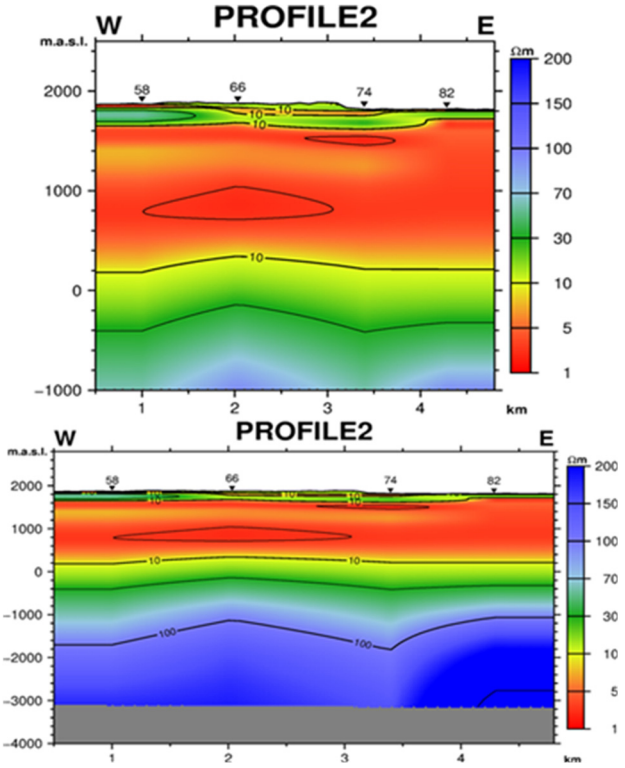

FIGURE 19: Resistivity cross-section along profile 2 for two depths 1,000 and 4,000 m b.s.l., respectively; its location is given in Figure 12. The grey body indicates the depth of resolution of the cross-section

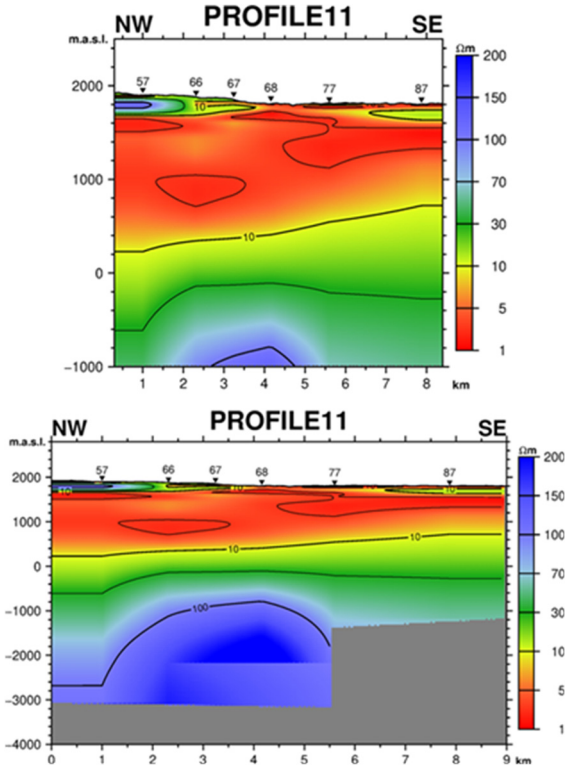

FIGURE 20: Resistivity cross-section along profile 11 for two depths 1,000 and 4,000 m b.s.l., respectively; its location is given in Figure 12. The grey body indicates the depth of resolution of the cross-section

Resistivity cross-section along profile 15 (Figure 21) runs from NW to SE. Its location is given in Figure 12. It cuts across the regional geological structures of the rift fault and the geothermal surface manifestations. Profile 15 is the longest profile in this study.

- A thin resistive surface layer (> 50 Ωm) getting thinner away from the centre, 200 m thick and at 1,900 m a.s.l.
- A 100 Ωm anomaly about 200 m thick below MT station 01, 02 and 03 in the NW part of the profile under the resistive surface layer.
- The very extensive high conductive layer (< 10 Ωm) about 700-1,400 m thick below the resistive surface layers, extending from 200 to 700 m below surface. This layer reaches to relatively great depth and great thickness at the center of the cross-section and is more elevated towards the SE.
- A deep lying resistive zone (> 100 Ωm) is found below sea level.

Resistivity cross-section along profile 19 (Figure 22) runs N-S across the regional geological structures of the rift fault. Its location is given in Figure 12.

- The very extensive high conductive layer (< 10 Ωm) is seen below a thin surface resistive layer with a thickness ranging from 1,000 m to 1,300 m.
- A thick deep laying resistive zone (> 100 Ωm) extends to great depth.

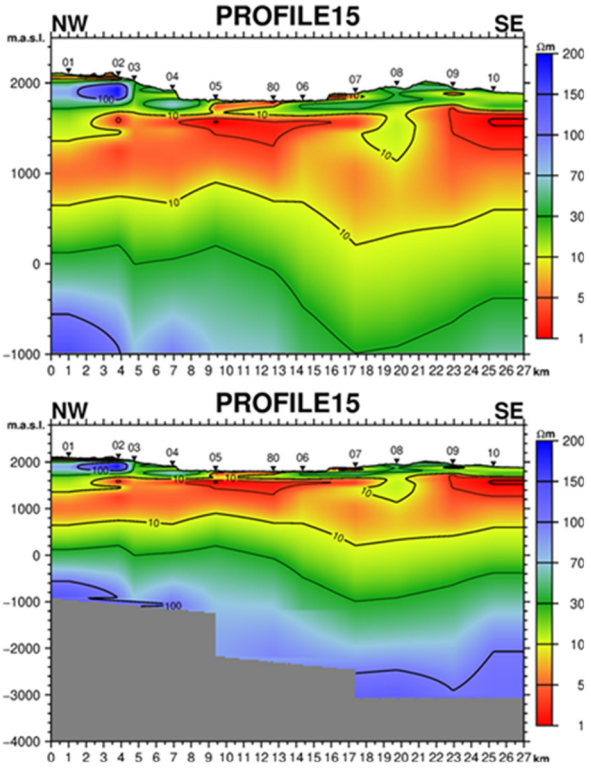

FIGURE 21: Resistivity cross-section along profile 15 for two depths 1,000 and 4,000 m b.s.l., respectively; its location is given in Figure 12. The grey body indicates the depth of resolution of the cross-section as the 1D models reflect different data quality

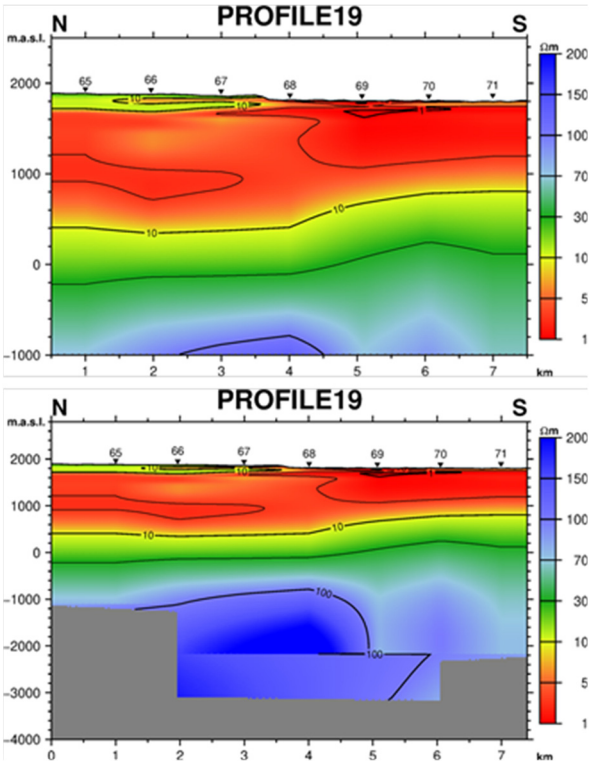

FIGURE 22: Resistivity cross-section along profile 19 for two depths 1,000 and 4,000 m b.s.l., respectively; its location is given in Figure 12. The grey body indicates the depth of resolution of the cross-section as the 1D models reflect different data quality

5.5 Horizontal resistivity cross-sections

Horizontal resistivity cross-sections (depth slices) based on the 1D models were produced using the TEMRESD program developed at ÍSOR (Eysteinsson, 1998). Here, four depth slices are presented and discussed showing resistivity at various depths with reference to sea level (Figure 23): At 1,800 m a.s.l., 1,000 m a.s.l, at sea-level and 500 m b.s.l. More depth maps are given in Appendix III in the Appendices report (Mengesha Negatue, 2021).

A pronounced up-doming low resistivity area (< 5 Ωm) is clearly seen around the geothermal surface manifestations at 1,800 m a.s.l. and 1,000 m a.s.l. (upper part of Figure 23), stretching to the north and east. The anomaly is probably connected to an up-flow of geothermal fluid and the associated smectite low-temperature alteration minerals (see section 3.5). The low resistivity is most likely caused by a combination of the smectite alteration minerals and saline sediments.

A high resistivity area (70-100 Ωm) is observed in the northwest part of the study area at sea level (Figure 23, lower figure to the left). The discontinuity in the Debre zait Silti graben suggests that the NE-SW fault system associated with Debre zait Silti and the transverse NW-SE older rift structure

control the magmatism (heat source). Ashute is characterized by recent and sub-recent basalt flows, phreatomagmatic deposits and a volcanic crater lake in which basalt is intensively weathered from bottom to the top of the crater. The high resistivity mapped around Ashute could be due to the recent and sub recent basalt flows.

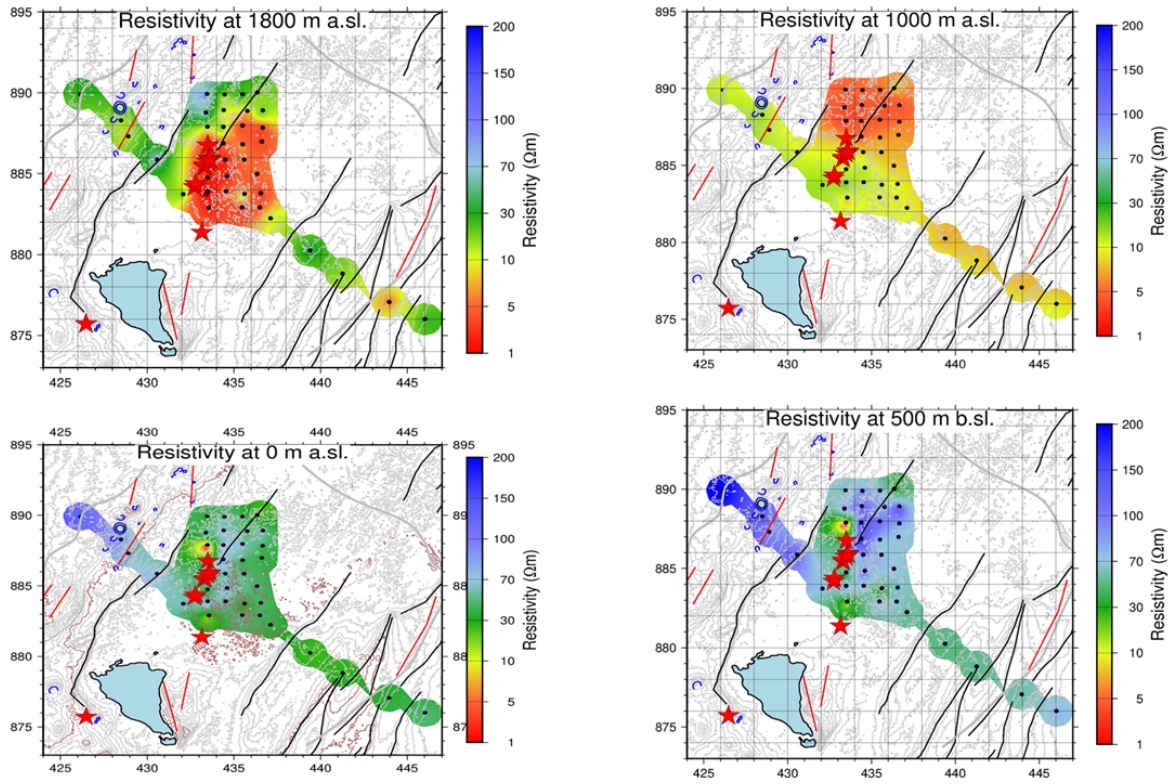

FIGURE 23: Horizontal resistivity cross-sections (depth slices) at various depths with reference to sea level: 1,800 m a.s.l., 1,000 m a.s.l., at sea-level and 500 m b.s.l. The thick grey lines are the accessible roads and field tracks, the black lines are the inferred faults mapped on the surface, and the red lines are the fissures. Black dots are MT stations and red stars are surface manifestations

6. STRIKE ANALYSIS

Geoelectrical strike analysis of MT data gives information about the 2D resistivity structure of the Earth by showing the direction in which the resistivity structure changes (Hersir et al., 2022). For a 2D Earth, the resistivity varies with depth and in one principal horizontal direction. The horizontal angle perpendicular to that direction is called the electrical strike and the angle it makes with geographical north is the Swift angle or *Z*-strike, Φ. As discussed in Section 3.7, it is possible to rotate the measured coordinate system of an MT sounding by mathematical means. If the earth is 2D and the coordinate system of the field layout/rotated layout has one axis parallel to the electrical strike direction, we get: $Z_{xx}=Z_{yy}=0$, but $Z_{xy}\neq Z_{yx}$. The electrical strike, *Z*-strike, can be determined by minimizing $|Z_{xx}|^2 + |Z_{yy}|^2$ with respect to Φ – the rotation of the coordinate system.

The penetration depth of MT soundings increases with increasing period as shown in Equation 10. The *Z*-strike depends on the period and, therefore, the electrical strike is depth dependent. The *Z*-strike is shown as a function of the period in Figure 13. There is, however, a 90° ambiguity in the strike angle determined by the impedance tensor. Therefore, the vertical component of the magnetic field H_z is often used for strike analysis; the Tipper or T-strike relates the vertical component of the magnetic field to its horizontal components (see Figure 13). The T-strike does not suffer the 90° ambiguity of the *Z*-strike.

The Tipper, T, is a complex (two component) vector and can be represented as two real vectors, or induction arrows, the real part and the imaginary part. The real part points away from a zone of low resistivity at sufficiently low frequencies and towards a zone of higher resistivity (Berdichevsky and Dmitriev, 2002; Hersir et al., 2022). The length of the arrows indicates the size of the resistivity contrast. For a 2D Earth model, the real and imaginary parts are co-linear and point perpendicular to the strike of the 2D geoelectrical structure (Berdichevsky and Dmitriev, 2002).

Figure 24 shows the induction arrows for the period of 1 s, corresponding to a depth of close to 1 km. Comparing the figure with the resistivity model in Figure 23 (1,000 m a.s.l.) we note that the real part of the induction arrows points away from the low resistivity body around the surface manifestations. Therefore, the strike analysis – induction arrows – are in good agreement with the resistivity model. Figure 25 shows a rose diagram of the T-strike for the period 1-10 s, corresponding to a depth of a little

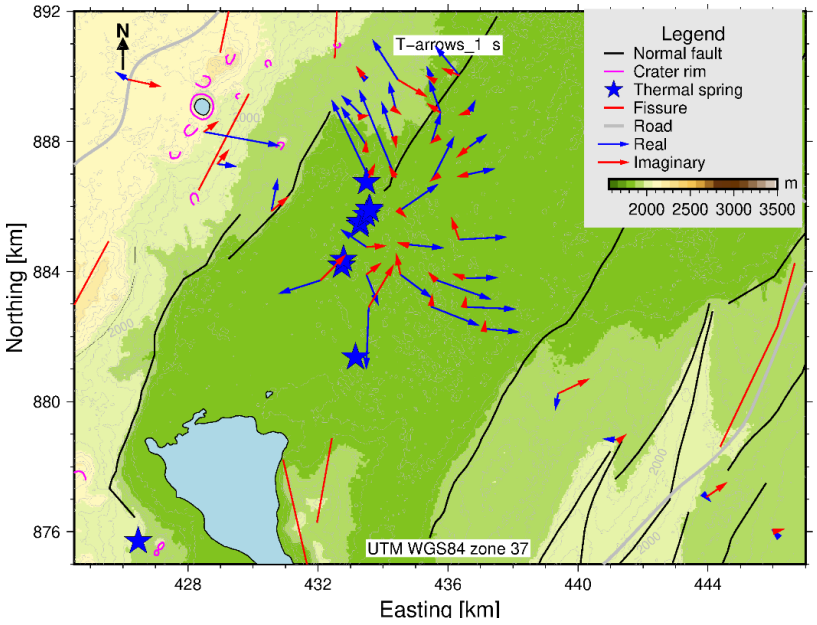

FIGURE 24: Induction arrows for the period of 1 s; blue arrows are the real part and red arrows the imaginary part. Geothermal surface manifestations and geological structures are also shown

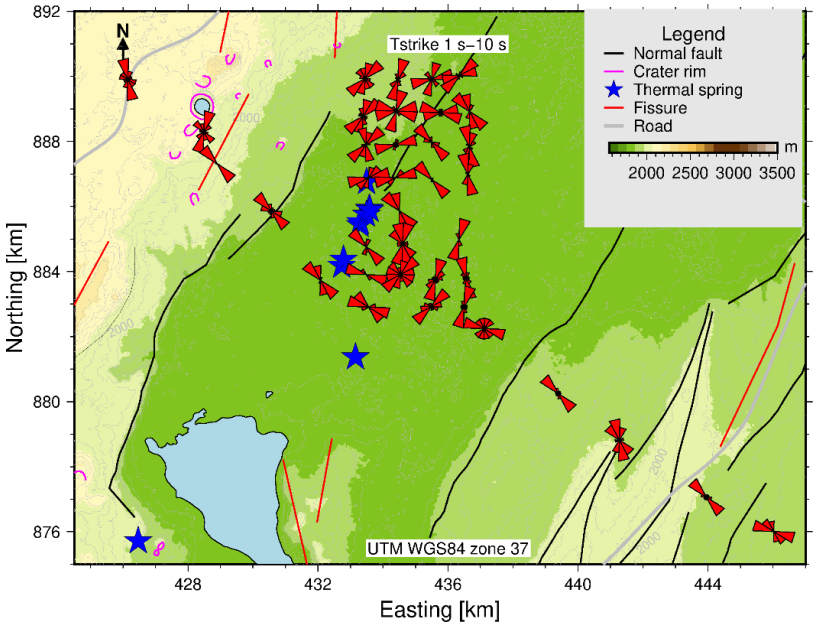

FIGURE 25: A rose diagram of the T-strike at 1-10 s. Geothermal surface manifestations and geological structures are shown as well

more than 1 km. The T-strikes are parallel to the low resistivity body around the surface manifestations in the resistivity model as shown in Figure 23, again a good agreement. The T-strikes to the NW and SE of the surface manifestations indicate a definite NW-SE lying resistivity contrast in these areas (Figure 25).

7. CONCLUSION

In this project, 38 MT/TEM soundings from the Butajira Silti Ashute area have been processed and 1D jointly inverted. The results are presented here as 1D resistivity models for each sounding pair and as both vertical and horizontal (depth slices), pseudo 2D resistivity cross-sections. The results are compared with the geological findings and the geothermal surface manifestations. The irregular nature of the orientation of the resistivity contour lines at different depth levels suggests that the Butajira prospect Ashute field is structurally complex, as indicated by the presence of the different orientations of the faults and fractures in the area.

The Ashute area is characterized by a shallow lying conductive layer with resistivity values less than 5-10 Ωm and an average thickness of about 1,200 to 1,600 m. It reaches down to a depth of 200 to 600 m a.s.l. The subsurface is composed of volcanic sediments including lithified ash, fine to coarse grained sandstone, well laminated conglomerate and debris or lahar. The clasts consist mostly of pyroclastic material derived from a silicic center in the south. The low resistivity is probably caused by the saline sediments and/or smectite low temperature hydrothermal alteration but most likely a combination of both.

Below the low resistivity, high resistivity of more than 70 Ωm is found, which presumably is related to the basement, fractured basalt and scoria. This high resistivity likely reflects the influence of major fault systems, the tectonic trend of the Debre zait Silti rift graben and the Main Ethiopian Rift (MER).

Presumably, geothermal fluid at depth rises to a shallow level along the NE-SW discontinuity and NW-SE structures, flowing laterally and enriching the shallow permeable formation, and appearing as thermal manifestations in the field.

Electrical strike analyses of the MT data using the vertical component of the magnetic field for different frequencies (depth levels) are in good agreement with the 1D resistivity model and support it.

8. RECOMMENDATIONS

A thorough and extensive resistivity study of the Butajira Silti Ashute area applying MT and TEM soundings as well as repeating bad data quality stations from previous studies is essential. Measurements should be done on a grid covering an area well outside the already recognized geothermal area. In particular, adding more stations around the area of geothermal surface manifestations to confirm the extension of the up-doming clay cap and the mapped fault zone which was observed to continue towards the Ashute hot springs is necessary.

1D joint inversion of the MT and TEM data and preferably 3D inversion of the static shift corrected MT data should be performed. The 3D inversion gives better resolution and shows more details.

Systematic structural geological mapping of the area is recommended to reduce uncertainties in the locations of mapped faults and other tectonic features. Most of the currently mapped faults are inferred or seen as lineaments in the geologic data. A gravity survey might well give additional information about the subsurface geological structure and is recommended as well.

Finally, all geoscientific results should be gathered into a conceptual model of the geothermal area.

ACKNOWLEDGEMENTS

I would like to thank my employer institution, the Geological Survey of Ethiopia (GSE), for allowing me to attend this six-month training. I sincerely would like to thank the Icelandic government, GRÓ GTP and its staff for giving me this full scholarship opportunity to participate in the six-month training programme and get financial and technical support.

I am greatly indebted and have no words to describe my supervisor Gylfi Páll Hersir and co-supervisors, Ásdís Benediktsdóttir and Knútur Árnason, for their continuous support, sharing their experience, starting from the data acquisition to processing and interpretation of the MT/TEM data to achieve my goals. I would also like to thank the GRÓ GTP 6 months, MSc, and PhD fellows for their help and sharing their experience, helping me to face challenging times and for enjoying good times with me during the whole period of my study. My special thank also goes to my colleagues at the GSE for their encouragement and Birhan Abera for her continuous sharing of experience and support.

Finally, I would like to say thanks to my wonderful family especially my lovely wife Lidiya Challa who gave birth to my new bouncing baby boy with help of God while I was doing this project.

REFERENCES

Abebe, B., Acocella, V., Korme, T., and Ayalew, D., 2007: Quaternary faulting and volcanism in the Main Ethiopian Rift. *J. African Earth Sciences, 48,* 115–124.

Abebe, Z., Sinetibeb, Y., and Eshetu, A., 2017*: Surface geothermal exploration mapping of Butajira-Silti area.* Geological survey of Ethiopia (GSE), Ethiopia, unpublished internal report, 21 pp.

Abera Kebede, B., 2021: *The relationship between the Tulu Moye geothermal system, the Ziway-Asela area and the tectonic structure of the Ethiopian Rift.* University of Iceland, MSc thesis, GRÓ GTP, report 3, 84 pp.

Abera Kebede, B. and Mulugeta, N., 2017: *One-meter temperature survey at the Butajira geothermal field*. Geological Survey of Ethiopia, Ethiopia, unpublished internal report, 17 pp.

Archie, G.E., 1942: The electrical resistivity log as an aid in determining some reservoir characteristics. *Transactions of the American Institute of Mining, Metallurgical, and Petroleum Engineering, 146,* 54–67.

Árnason, K., 1989: *Central loop transient sounding over a horizontally layered earth.* Orkustofnun, Reykjavik, Iceland, report OS-89032/JHD-06, 129 pp.

Árnason, K., 2006a: *TemX, short manual.* ÍSOR – Iceland GeoSurvey, Reykjavík, Iceland, internal report, 17 pp.

Árnason, K., 2006b: *TEMTD, a program for 1D inversion of central-loop TEM and MT data*. ÍSOR – Iceland GeoSurvey, Reykjavík, Iceland, unpublished manual, 17 pp.

Árnason, K., Flóvenz, Ó.G., Georgsson, L., and Hersir, G.P., 1987: Resistivity structure of high-temperature geothermal systems in Iceland. *International Union of Geodesy and Geophysics (IUGG) XIX General Assembly*, *Vancouver, BC, Canada, Abstract V,* 477.

Berdichevsky, M.N. and Dmitriev, V.I., 2002: Magnetotellurics in the context of the theory of ill-posed problems. *Soc. of Expl. Geophys*., *11,* 137-138.

Boccaletti, M., Bonini, M., Mazzuoli, R., Abebe, B., Piccardi, L., and Tortorici, L., 1998: Quaternary oblique extensional tectonics in the Ethiopian Rift (Horn of Africa). *Tectonophysics, 287,* 97–116.

Chave, A.D., and Smith J.T., 1994: On electric and magnetic galvanic distortion tensor decompositions. *Geophys. Res*., *99,* 4669–4682.

Chave, D.A., Robe, L.E., Ian, J.F, Alan, G.J., Randall, L.M., William, L.R., Ari, V., and Peter, W., 2012: Introduction to the magnetotelluric method. In: Chave, A.D. and Jones, A.G. (eds.), *The magnetotelluric method*. Cambridge University Press, 1-14.

Dakhnov, V.N., 1962: *Geophysical well logging: The application of geophysical methods; electrical well logging.* Colorado School of Mines, CO, United States, 445 pp.

Didas, M.M., 2018: 1D joint inversion of MT and TEM data from Ngozi geothermal prospect, SW Tanzania – an integrated interpretation of geoscientific results. Report 13 in: *Geothermal training in Iceland 2018*. UNU-GTP, Iceland, 141-186.

ELC, 1986: *Exploitation of Langano-Aluto geothermal resources.* Electroconsult (ELC), feasibility report, Milano, Italy.

Eysteinsson, H., 1998: *TEMMAP and TEMCROSS plotting programs*. ÍSOR – Iceland GeoSurvey, Reykjavík, Iceland, unpublished programs and manuals.

Flóvenz, Ó.G., Hersir, G.P., Saemundsson, K., Ármannsson, H., and Fridriksson, Th., 2012: Geothermal energy exploration techniques. In: Sayigh, A. (ed.), *Comprehensive renewable energy,* Elsevier, Oxford, United Kingdom, 51-95.

Flóvenz, Ó.G., Spangenberg, E., Kulenkampff, J., Árnason, K., Karlsdóttir, R., and Huenges, E., 2005: The role of electrical interface conduction in geothermal exploration. *Proceedings World Geothermal Congress 2005*, *Antalya, Turkey,* 9 pp.

Hailegiorgis Abebe, G., 2018: Processing and joint 1D inversion of MT and TEM data from Alallobeda geothermal field NE-Ethiopia. *Proceedings 6th African Rift Geothermal Conference, Addis Ababa, Ethiopia*, 13 pp.

Hailegiorgis Abebe, G. and Hersir, G.P., 2020: 1D joint inversion of electromagnetic data from Meteka geothermal prospect, Ethiopia. *Proceedings, 8th African Rift Geothermal Conference, Nairobi, Kenya*, 9 pp.

Hersir, G.P. and Árnason, K., 2009: Resistivity of rocks. *Paper presented at "Short Course on Surface Exploration for Geothermal Resources", organized by UNU-GTP and LaGeo, Ahuachapán and Santa Tecla, El Salvador,* 8 pp.

Hersir, G.P., Gudnason, E.Á., and Flóvenz, Ó.G., 2022: Geophysical exploration techniques. In: Letcher, T. (ed.), *Comprehensive renewable energy – 2nd edition, Vol 7,* Elsevier, Oxford, United Kingdom, 26-79.

Kebede, S., 2016: Country update on geothermal exploration and development in Ethiopia. *Proceedings 6th African Rift Geothermal Conference, Addis Ababa, Ethiopia,* 8 pp.

Keller, G.V. and Frischknecht, F.C., 1966: *Electrical methods in geophysical prospecting.* Pergamon Press Ltd., Oxford, United Kingdom, 527 pp.

Kristmannsdóttir, H., 1979: Alteration of basaltic rocks by hydrothermal activity at 100-300°C. *Developments in sedimentology, 27,* 359-367.

Mengesha Negatu, K., 2021: Appendices to the report "Butajira geothermal prospect in Silti zone, Southern Ethiopia: 1D joint inversion of MT and TEM resistivity data – Geological and geothermal significance". Report 16 in: *Geothermal Training in Iceland 2021*. GRÓ GTP, Iceland, appendices, 140 pp.

Mengiste, A., Mengesha, K., Burusa, G., Abera, F., Yismaw, A., and Wondifraw, T., 2018: 1D and 2D inversions of magnetotelluric data from Butajira geothermal field, Southern Ethiopia. *Proceedings 7th African Rift Geothermal Conference, Kigali, Rwanda,* 13 pp.

Mohr, P.A., 1983: Ethiopian flood basalt province. *Nature, 303,* 577-584.

Park, S.K. and Livelybrooks, D.W., 1989: Quantitative interpretation of rotationally invariant parameters in magnetotellurics. *Geophysics, 54(11),* 1483-1490.

Phoenix, 2005: *Data processing user guide, SSMT2000, NPIPlot, MTEditor, synchro time series View.* Phoenix Geophysics Ltd., Toronto, Canada, 212 pp.

Phoenix, 2018: *Phoenix Geophysics,* website: *www.phoenix-geophysics.com/home*

Quist, A.S., and Marshall, W.L., 1968: Electrical conductances of aqueous sodium chloride solutions from 0 to 800°C and at pressures to 4000 bars. *J. Physical Chemistry, 72,* 684-703.

UNDP, 1973: *Geology, geochemistry, and hydrology of hot springs of the East African Rift System within Ethiopia.* United Nations Development Programme, December report DD/SF/ON/11, New York, NY, United States.

Ward, S.H. and Wannamaker, P.E., 1983: *The MT/AMT electromagnetic method in geothermal exploration*. United Nations University Geothermal Training Programme, Reykjavík, Iceland, report 5, 107 pp.

WoldeGabriel, G., Aronson, J.L., and Walter, R.C., 1990: Geology geochronology and rift basin development in the central sector of the Main Ethiopian Rift. *Geological Society of America, 102,* 439–458.

Wondifra Tadesse, T., 2018: 1D inversion of magnetotelluric data from Ashute, Butajira geothermal prospect, SE-Ethiopia and its geothermal implications. Report 29 in: *Geothermal training in Iceland 2018*. United Nations University Geothermal Training Programme, Reykjavík, Iceland, 577-603.

Zonge, 2018: *Transient electromagnetic or time-domain EM (TEM)*, website: *www.zonge.com/geophysical-methods/electrical-em/tem/*